Showcasing the work on binding of ruthenium intercalators to DNA by Anna K. F. Mårtensson and Per Lincoln, Department of Chemical and Biological Engineering, Chalmers University of Technology, Sweden.

Binding of Ru(terpyridine)(pyridine)dipyridophenazine to DNA studied with polarized spectroscopy and calorimetry

Achiral Ru(tpy)(py)dppz^{2+} intercalated into the minor groove of DNA has similar intermolecular interactions as opposite enantiomers of its structural isomer, the "light-switch" complex Ru(bpy)$_2$dppz^{2+}.

ROYAL SOCIETY OF CHEMISTRY

www.rsc.org/dalton

PAPER

Binding of Ru(terpyridine)(pyridine)-dipyridophenazine to DNA studied with polarized spectroscopy and calorimetry†

Anna K. F. Mårtensson and Per Lincoln*

Linear and circular dichroism (LD and CD) spectroscopy as well as isothermal titration calorimetry (ITC) have been used to investigate the interaction of Ru(tpy)(py)dppz^{2+} (tpy = 2,2′:6′,2″-terpyridyl; py = pyridine; dppz = dipyrido[3,2-a:2′3′-c]phenazine) with DNA, providing detailed information about the DNA binding thermodynamics and binding geometry of the metal complex. Flow LD, CD and isotropic absorption indicate that Ru(tpy)(py)dppz^{2+} bind to DNA from the minor groove with the dppz ligand intercalated between base pairs, very similar to its chiral structural isomers Δ- and Λ-Ru(bpy)$_2$dppz^{2+} (bpy = 2,2′-bipyridine). A simple cooperative binding model with one binding geometry provide an excellent fit for calorimetric and absorption titration data. The values of the neighbor interaction thermodynamic parameters for Ru(tpy)(py)dppz^{2+} suggest that complexes bound contiguously prefer to have their tpy ligands oriented towards the same strand.

Introduction

DNA-binding drugs are small molecules that recognize and interact with specific DNA sites. Many of the chemotherapeutic anticancer agents currently in use fall under this category with cisplatin being the most prevalent example.[1] DNA intercalators that unwind DNA in order to π-stack between two base pairs have shown cytotoxicity towards cancerous cells but are often of limited therapeutic use due to their lack of specificity and frequent side effects. After the pioneering work by Barton and coworkers on the selective DNA binding of substitution-inert trisphenanthroline complexes of ruthenium, there has been an increasing interest in octahedral transition metal complexes.[2] The discovery of the "light switch" complexes Ru(phen)$_2$dppz^{2+} and Ru(bpy)$_2$dppz^{2+} (phen = 1,10-phenanthroline; bpy = 2,2′bipyridine; dppz = dipyrido[3,2-a:2′3′-c]-phenazine) lead to the synthesis of many variations of dppz-ruthenium-centered tris-bidentate structures with the potential as biosensors and therapeutic agents.[3] Interestingly, the two ruthenium complexes that have reached clinical trials have substitution-labile ligands and a proposed mode of action completely different to DNA intercalation.[4]

Spectroscopic and biophysical methods have established that it is the dppz ligand in tri-bidentate complexes that is intercalated between the base pairs of the DNA, and this has recently been confirmed by several X-ray crystal structures.[5] Compared to the intense research on the brightly luminescent bipyridine and phenanthroline complexes, the very low quantum yield at room temperature has led to less interest for ruthenium dppz complexes carrying the tridentate tpy ligand (tpy = 2,2′:6′,2″-terpyridyl), despite the fact that the absence of a stereocentre at the metal when coordinated to a tridentate ligand eliminates the need of separating Δ and Λ racemic mixtures characteristic of tris-bidentate systems. The main focus has been on tpy-based complexes with reactive oxoruthenium(ɪᴠ) functionality that cleaves DNA by oxidation of guanine and the 1′-deoxyribose hydrogen.[6] However, not until recently has the single free coordination site left on the metal atom been recognized as a potential way of fine-tuning complex–DNA interactions, either by improving the DNA cleaving ability,[7] or as a novel light-activated drug delivery system.[8] Although some spectrophotometric studies have aimed at the DNA binding mode of tpy-based complexes to DNA,[9] a definite proof of the binding geometry has not yet been obtained.

Our group has previously determined that the tris-bidentate complexes affect each other, either cooperatively or anti-cooperatively, when interacting with a DNA-polymer *via* intercalation.[10] A binding model that gives a satisfactory fit to the data needs two distinct binding modes, one symmetrical (perpendicular) and one unsymmetrical (polar). This model with two modes of binding is supported by the crystallographic study by

Department of Chemical and Biological Engineering, Chalmers University of Technology, SE-41296 Gothenburg, Sweden. E-mail: marann@chalmers.se, lincoln@chalmers.se
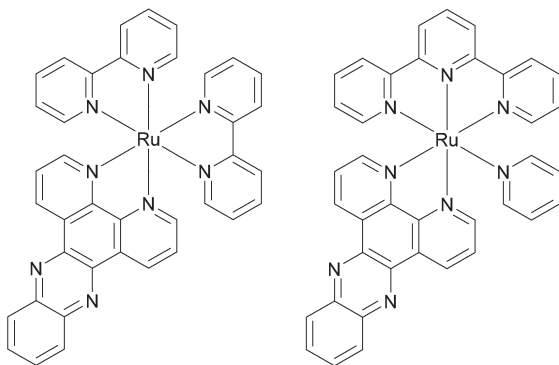
Scheme 1

Scheme 1 Structures of ruthenium complexes Ru(bpy)$_2$dppz^{2+} (left) and Ru(tpy)(py)dppz^{2+} (right).

Fig. 1 Absorption spectra of Ru-tpy (black) and ΔRu-bpy (red) (14 μM) in 150 mM NaCl solution (dotted line) and in presence of AT-DNA (138 μM nucleotides) (solid line). The gray line shows AT-DNA only.

Niyazi *et al.* (2012) where a symmetric and a non-symmetric intercalation geometry was found for Λ-Ru(phen)$_2$dppz^{2+}.[5f]

In this study, we have carried out spectrophotometric and calorimetric measurements in order to determine the binding geometry and thermodynamic characteristics of Ru(tpy)(py)-dppz^{2+} (Ru-tpy, see Scheme 1). To simplify the system by avoiding effects from DNA sequence heterogeneity, and to compare with an earlier study,[10] we chose to primarily study the interaction of poly(dAdT)$_2$ (AT-DNA). However, since the AT-DNA was too short to orient in the flow cell for the linear dichroism study, we used calf thymus DNA (ctDNA) instead. We wanted to characterize a tpy/dppz ruthenium complex in its simplest form, and for the purpose of comparison, a pyridine (py) ligand was attached to the single coordination site, making the complex an achiral structural isomer of the original "light-switch" complex Ru(bpy)$_2$dppz^{2+} (Ru-bpy). Once we have gained more understanding in how this mononuclear complex interacts with DNA, the substituents of this single coordination site could be varied to optimize properties that would make it and its binuclear derivatives more suitable as metallo-pharmaceuticals.

Results

Absorption

The absorption spectra of ΔRu-bpy and Ru-tpy in the absence and presence of AT-DNA at [base pairs]/[Ru] ratio of 5 are illustrated in Fig. 1. The broad band system centered at about 440 nm for ΔRu-bpy and 475 nm for Ru-tpy is attributed to the metal to ligand charge transfer (MLCT) transitions, which in the presence of AT-DNA show a slight hypochromicity and red shift for both complexes. The characteristic 372 nm band, assigned to the lowest π→π* transitions of the dppz chromophore is almost identical for both Ru-tpy and ΔRu-bpy, and in presence of AT-DNA there is also a very similar pronounced hypochromicity and red-shift (see Fig. 1 and Fig. S1 in ESI†).[11] For Ru-tpy, the most intense band outside the overlapping DNA absorption is the band at about 310 nm, which is assigned to the long-axis polarized lowest π→π* transition of
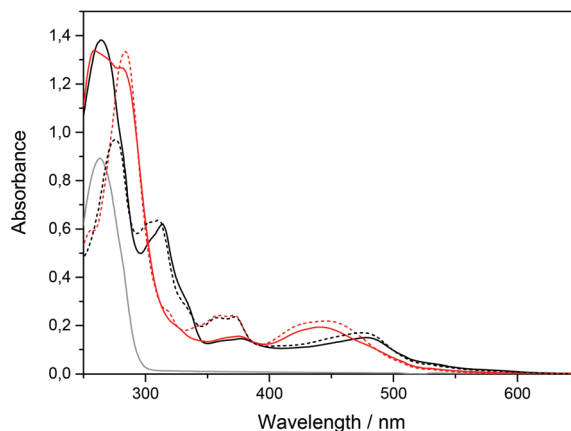
the tpy chromophore.[12] This peak shows a red-shift of about 5 nm and in contrast to the 372 nm dppz band, only a slight hypochromicity at DNA binding, indicating that of the two large ruthenium ligands in Ru-tpy, the dppz ligand is the one that has the closest interaction with the nucleobases. As shown by titrating a constant concentration of Ru-tpy with AT-DNA (see Fig. S2 in ESI†), the hypochromicity of the dppz-band at 372 nm for Ru-tpy remains virtually constant at ratios [base pairs]/[Ru] > 2, whereas the initial hypochromicity in the 310 nm band is somewhat reduced at higher ratios.

Circular dichroism

A pure enantiomer of a chiral ruthenium complex, such as Ru-bpy, will show a strong intrinsic CD signal when free in aqueous solution, but Ru-tpy, which is an achiral complex will show zero CD signal under the same conditions. However, for both chiral and achiral molecules, binding to DNA can lead to a proper induced circular dichroism signal (proper ICD) by perturbation of the chromophores of the bound molecule by the chiral arrangement of the nucleobase chromophores. Here the magnitude and the sign of the ICD will mainly be dictated by the distances and angles between the interacting electronic transition dipole moments, and similar geometries are expected to give rise to similar ICD-patterns even for opposite enantiomers. In addition, for chiral molecules, changes merely in position and intensity of the intrinsic CD bands themselves, caused by the interaction with DNA, will add an apparent ICD contribution, but this will be characterized by a mirror-image like pattern for opposite enantiomers with similar binding geometries. Changes in CD were monitored upon addition of ΔRu-bpy, ΛRu-bpy, and Ru-tpy to a [base pairs]/[Ru] ratio of 5. In order to compare the ICD spectra of the complex–DNA interactions, the spectrum of the DNA and the spectrum of the free complex were subtracted from the spectrum in the presence of DNA. Fig. 2 shows the ICD of all three complexes as well as the CD spectrum of the AT-DNA. The general shape of the ICD below 290 nm is quite similar for all three complexes:
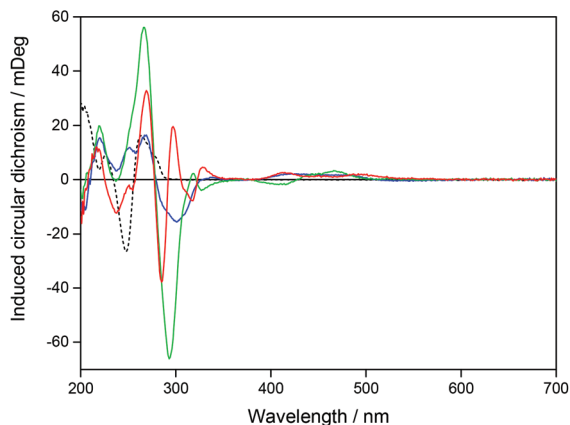
Fig. 2 Induced CD for Ru-tpy (blue), ΔRu-bpy (green), and ΛRu-bpy (red) after mixing with AT-DNA. The black dashed line shows the CD signal for AT-DNA in a 150 mM NaCl solution. The concentrations of complex and DNA were 14 and 138 μM respectively.

Fig. 4 Resolved spectra of the x and y (red) and the z (blue) polarized absorption bands of Ru-tpy bound to ctDNA. The Y-axis units are $\varepsilon/(1000\ M^{-1}\ cm^{-1})$. The arrows on the molecular structure of the complex show the direction of the x and z transition moments.

a negative band between 275 and 290 nm and a positive band at about 260 nm, indicative of a proper ICD mechanism, while the general mirror-image relationship of the ICD curve >290 nm for Δ- and ΛRu-bpy suggests the predominance of an apparent ICD mechanism in this region. Titration of a solution with constant concentration of Ru-tpy shows an almost invariant CD spectrum >300 nm for [base pairs]/[Ru] > 2, similar to the results of the corresponding absorption titration (see Fig. S3 in ESI†).

Linear dichroism

Fig. 3 shows the LD spectra for Ru-tpy in ctDNA solution at [base pairs]/[Ru] ratios 8, 4 and 2. The ctDNA concentration remained constant at 270 μM nucleotides. The reduced LD (LD^r), which is the LD divided by the isotropic absorbance, is very similar for all [base pairs]/[Ru] ratios, indicating little or no change in the geometric orientation at higher saturation levels (see Fig. S4 in ESI†). Thus, the conditions were fulfilled
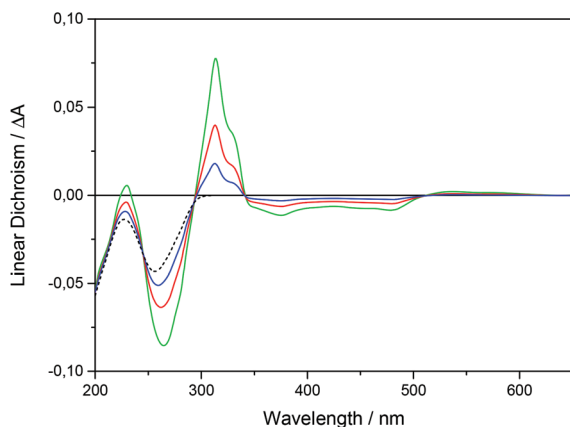
for determining the orientation factor S using eqn (5), (8) and (11) (See Theory and methods section below) using the LD spectra of free DNA (L_0) and at ratios 8 (L_1) and 4 (L_2). The relative values $S_1/S_0 = 1.06$ and $S_2/S_0 = 1.16$ indicate that the DNA with bound Ru-tpy becomes better oriented, as earlier found for Δ- and ΛRu-bpy.[11a] Finally **b**, the pure (without DNA contribution) Ru-tpy LD spectrum, at perfect orientation and 10 mm optical path-length, was calculated as $\mathbf{b} = c_2^{-1}(S_2^{-1}L_1 - S_0^{-1}L_0)$. The weights w_1 and w_2 in eqn (6) were varied manually until the dppz band at 375 nm vanished in component $\mathbf{e}_1$ and the sharp tpy absorption band at 310 nm vanished in component envelope spectra $\mathbf{e}_2$, as shown in Fig. 4. The optimal weight values were $w_1 = 3 \pm 0.5$ and $w_2 = -1.5 \pm 0.3$, the theoretical limits for parallel and perpendicular orientation of a transition dipole moment relative to the orientation axis. Thus, the results show that the tpy long-axis (z) is aligned along and the dppz long-axis (x) perpendicular to the DNA helix axis, which, since the dppz ligand lies in the x,y plane, is consistent with intercalation of the dppz ligand in-between the base pairs.

Binding isotherms

ITC profiles for the binding of Ru-tpy to AT-DNA at 20, 25, and 30 °C are shown in Fig. 5 and for comparison, the corresponding ITC-profiles for Δ- and ΛRu-bpy from Andersson *et al.* (2013).[10] Ru-tpy shows a similar overall shape with a gradually increasing exothermic enthalpy until a negative maximum is reached at [Ru]/[base pairs] = 0.4–0.5, somewhat higher than for the other two complexes. The initial slope of the ITC profile is in contrast to the initial constant part of the sigmoidal curve expected for the simple binding as indicated above by absorption, circular dichroism and linear dichroism spectroscopies, where the spectra of Ru-tpy in the presence of DNA were found to be practically invariant with binding ratio. This suggests that intermolecular interactions between bound molecules must contribute to the binding enthalpy also for Ru-tpy, as earlier concluded for Δ- and ΛRu-bpy.[10] This

Fig. 3 Linear dichroism spectra of Ru-tpy in the presence of ctDNA at [base pairs]/[Ru] ratios 8 (blue), 4 (red) and 2 (green) in 10 mM NaCl solution, as well ctDNA alone (dotted). The concentration of ctDNA is 270 μM nucleotides.
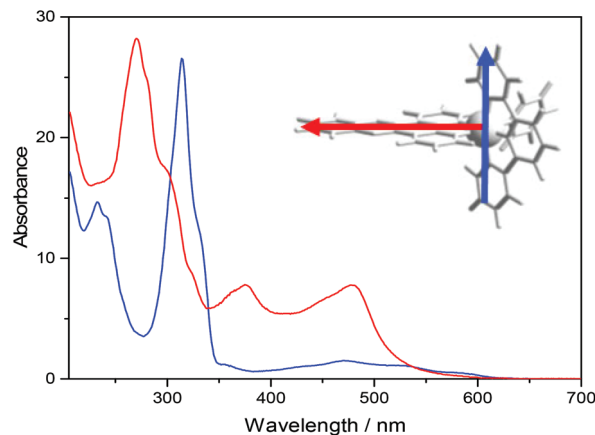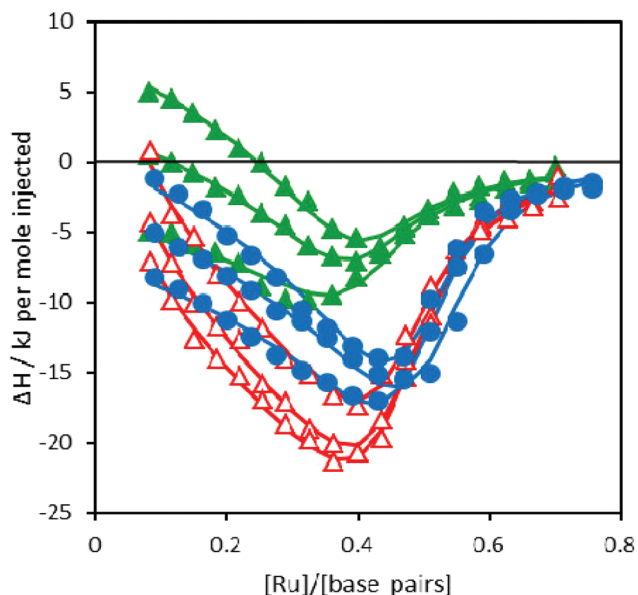
Fig. 5 ITC profiles with fitted traces for the binding of Ru-tpy (●), ΔRu-bpy (▲), and ΛRu-bpy (△) to AT-DNA in 150 mM NaCl solution at 20, 25, and 30 °C. Symbols indicate the normalized heat absorbed or evolved upon sequential injections (2 μL) of complex into the 206 μL cell containing the DNA. The data has been corrected for heat of complex dilution. The corresponding ITC-profiles for Δ- and ΛRu-bpy are from Andersson *et al.* (2013).[10]
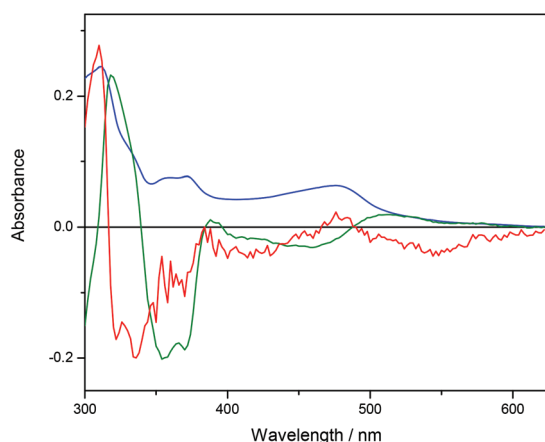

Fig. 6 The **U**-vectors corresponding to the first three singular values (s_1 blue, s_2 green, s_3 red) from the titration of Ru-tpy to a constant concentration of AT-DNA in 150 mM NaCl at 25 °C.

observation prompted us for a more thorough analysis of the spectroscopic changes, and absorption spectra were collected for addition of Ru-tpy to a constant concentration of AT-DNA at 25 °C.

The data (shown in Fig. S5 in ESI†) were analyzed with singular value decomposition (SVD) as described in Theory and methods. The first three (normalized) singular values were s_1 = 100, s_2 = 2.45 and s_3 = 0.23, and the corresponding columns of **U** and **V** are plotted in Fig. 6 and 7, respectively.
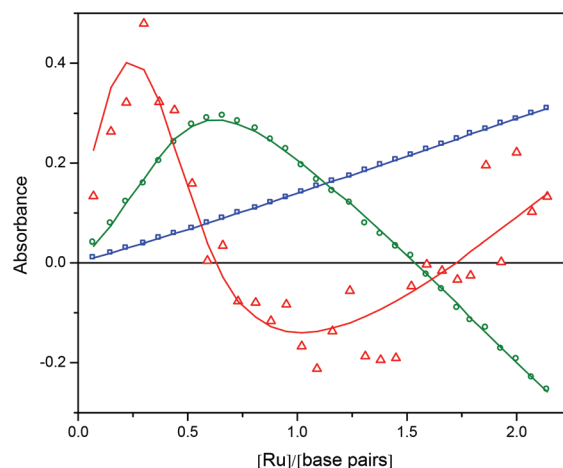

Fig. 7 The **V**-vectors corresponding to the first three singular values (s_1 blue squares, s_2 green circles, s_3 red triangles) from the titration of Ru-tpy to a constant concentration of AT-DNA in 150 mM NaCl at 25 °C. The fit of the model is shown as solid curves.

Fig. 8 Calculated absorption spectra for unbound complex (blue), bound complex with at most one neighbor (green) and bound complex with at least one neighbor (red).

Column **4** in **U** and **V** (shown in Fig. S6 and S7 in ESI†) were much less structured and were judged to be insignificant, although the fourth singular value (0.18) was close to the third.

Ru-tpy ITC and absorption data could be excellently globally fitted with the classical McGhee–von Hippel cooperative binding model (see Theory and methods), and the best fit to the data are shown with solid lines in Fig. 5 and 7. Fig. 8 shows the calc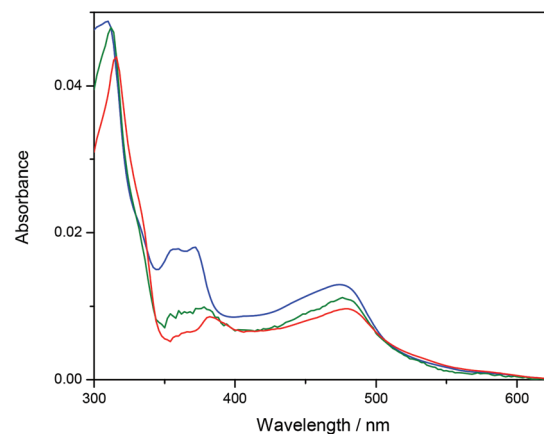ulated absorption spectra for free complex, bound complex with at most one neighbor and bound complex with at least one neighbor. For comparison, the model was also used to fit the ITC data for ΔRu-bpy and ΛRu-bpy, as shown in Fig. 5. A linear fit to the calculated $\Delta H°$ values as a function of temperature is shown in Fig. 9, and Table 1 gives the parameters and derived thermodynamic data.
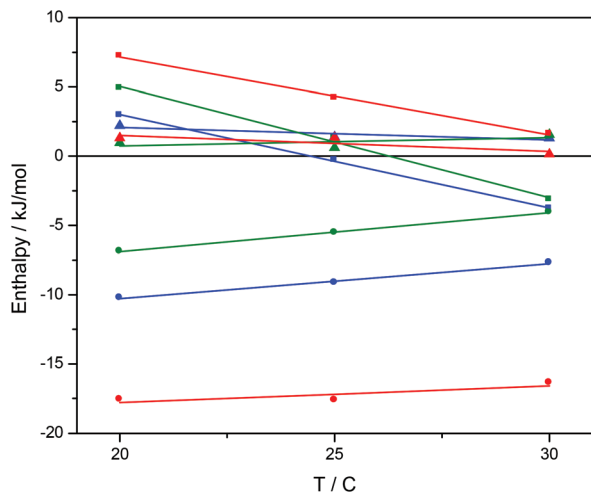
Fig. 9 The standard binding enthalpy ΔH_b° (■), standard nearest neighbor interaction enthalpy ΔH_{nn}° (●), and $\Delta H_{baseline}^\circ$ (▲) for binding of Ru-tpy (blue), ΔRu–bpy (green), and ΛRu–bpy (red) to AT-DNA in 150 mM NaCl. The slopes of the fitted lines correspond to the ΔC_p for the reactions.

Table 1 Binding constants K, cooperativity parameters y, and binding site sizes n that gave the best fit to experimental data, and the derived thermodynamic parameters for the intrinsic binding at 20 °C

Sample	K^a	y	n	$\Delta H_b^{\circ\,b}$	$\Delta H_{nn}^{\circ\,b}$	$\Delta C_{pb}^{\,c}$
Ru-tpy	1	2.8	2.0	3.0	−10.2	−680
ΔRu–bpy	0.9	1	2.2	4.3	−6.9	−800
ΛRu–bpy	0.06	5.5	2.3	7.2	−17.6	−560

^{a} $K/10^6$ M^{-1}. ^{b} ΔH°/kJ mol^{-1}. ^{c} ΔC_p/J mol^{-1} K^{-1}.

Discussion

Recently, high-resolution structures and calorimetric studies have highlighted ligand–ligand interactions as an explanation to the complex thermodynamical and photophysical behavior of DNA-bound Ru(L)$_2$dppz complexes.[5d–f,10] To further investigate the role of the ancillary L ligands, we chose to study the terpyridine/pyridine Ru-dppz complex Ru-tpy, an achiral isomer of Ru(bpy)$_2$dppz formally made by breaking the pyridine–pyridine bond of one bpy unit and joining it to the second (see Scheme 1).

Absorption spectroscopy shows that the spectral changes of the dppz ligand bands are virtually identical for ΔRu–bpy and Ru-tpy upon binding to DNA, giving a first indication that the binding mode of the two isomers are similar. Circular dichroism spectroscopy shows a negative induced CD band in the long-axis polarized tpy band at 300 nm, similar to the negative induced CD shown for Δ- and ΛRu–bpy in their long-axis polarized bpy band at 290 nm, as could be expected for electronic transitions positioned in the minor groove close to parallel to the helix axis.[13] Both absorption and CD are practically invariant with binding ratio, although a small perturbation of the tpy-band at 310 nm can be observed at binding ratios close to

saturation in both CD and absorption spectra. Likewise, linear dichroism spectra were found to be invariant with binding ratio too, allowing determination of the orientation factor S and a quantitative analysis of the angular binding geometry. In contrast to the Ru(L)$_2$dppz complexes, where major transition moment directions have oblique angles to the plane of the dppz ligand, in Ru-tpy the long-axis polarized tpy transition is perpendicular to the dppz plane. With a weight $w_1 = +3 \pm 0.5$ we find that it is almost perfectly parallel oriented to the DNA helix axis, and the dppz long axis polarized transition, with weight $w_2 = -1.5 \pm 0.3$, perpendicularly oriented, the geometry expected for intercalation of the dppz ligand in-between the base pairs of DNA. In contrast to the very minute differences in absorption, CD and LD spectra at different binding ratios, the calorimetric titration show strong effects on the heat of binding. We have previously been reported such non-classical ITC curves for Ru(L)$_2$dppz complexes (L = bpy or phen) and attributed them to an additional enthalpy contribution from interaction between neighboring complexes on the DNA.[10] In comparison to Δ- and ΛRu–bpy, Ru-tpy showed an ITC profile qualitatively most similar to the latter. Since a satisfactory global fit for the ITC and absorption experimental data of Ru-tpy could be obtained with the classical McGhee–von Hippel model with only one type of binding geometry, for comparison this model was also used to reanalyse our data for Δ- and ΛRu–bpy, which were originally fitted with a symmetrical and a pair of unsymmetrical intercalation geometries.[10] In this model (Model 3 in ref. 10), ligands bound with only one nearest-neighbor are assumed to have one distinct binding geometry (unsymmetrical), while ligands bound either isolated or with nearest-neighbors on both sides have a second binding geometry (symmetrical). As noted in our previous study, the fit of the simpler model to the ITC-data alone is excellent, but any attempt to rationalize the observed molar fractions of the short and the long excited state life-time fails. With the simple model, the apparent site sizes for Δ- and ΛRu–bpy were found to be 2.2 and 2.3, consistent with the neglect of the anti-cooperativity which is inherent in Model 3 for which the n parameters were found to be 2.0 and 1.8, respectively.[10] Interestingly, the binding site size parameter n was found to be 2.0 for Ru-tpy, indicating that the distinction between symmetrical and unsymmetrical intercalation geometries might be less pronounced for this complex. Although the low emission quantum yield of Ru-tpy bound to DNA precluded time-resolved luminescence measurements, the observation that spectra (absorption, CD, LD) change very little with binding density (see Fig. 3, S2 and S4†) support the conclusion that difference between intercalation geometries is small for Ru-tpy. The simple model has only one cooperativity parameter y, which is found to be 1 for ΔRu–bpy (i.e. non-cooperative binding) and 5.5 for ΛRu–bpy (cooperative binding); for Ru-tpy y = 2.8, in-between the values of the two Ru-bpy enantiomers. The intrinsic binding constant K is 10^6 M^{-1} for Ru-tpy, very similar to that of ΔRu–bpy, while K for ΛRu–bpy is almost 50 times smaller. The latter value is about 3 times smaller than that obtained with Model 3, however,

since simulated binding isotherms are the most sensitive to the value of the binding constant close to saturation, the best-fit value will normally be quite dependent on the binding model since the influence of the cooperativity parameters will differ.

The intrinsic binding enthalpy ΔH_b° is positive for all complexes at 20 °C, *i.e.* the binding in the absence of neighbor interactions is endothermic. The value of ΔH_b° is smaller for Ru-tpy than for either Δ- or ΛRu-bpy, but the temperature dependence is similar as evidenced by the negative ΔC_p-values of -680 ± 120 J K^{-1} M^{-1}. The nearest-neighbor interaction enthalpy ΔH_{nn}° is negative (*i.e.* exothermic) for all complexes, and exhibits a tendency similar to the cooperativity factor y, namely that the value for Ru-tpy is in-between the values for Δ- and ΛRu-bpy.

However, even if a simple, single binding geometry model is sufficient to model the binding data for Ru-tpy, the lack of a 2-fold axis of symmetry, in contrast to Δ- and ΛRu-bpy, make 2 types of neighbor interaction possible: either the tpy ligands of two consecutive complexes are oriented towards the same strand (T_{SS}, see Fig. 10) or they are oriented towards opposite (alternating) strands (T_{AS}). In comparison to Ru-bpy, neglecting the influence of the single pyridine ring of Ru-tpy, the alternating model (T_{AS}) would have intermolecular contacts resembling alternating Δ–Δ and Λ–Λ contacts, while the same-side model (T_{SS}) would everywhere have intermolecular contacts resembling Δ–Λ, comparable to that found in a recent X-ray crystal structure of Δ- and Λ-Ru-(phen)$_2$dppz simultaneously intercalated to a DNA hexamer duplex.[5e]

Since the same-side model T_{SS} has only one type of intermolecular contact (Δ–Λ), it is logically consistent with the simple one-geometry binding model, and also consistent with the assumption that Ru-bpy interactions model those of Ru-tpy, since 7.8, the square of the Ru-tpy y value of 2.8, is larger than the product 5.5 of the corresponding Δ–Δ and Λ–Λ y values for Ru-bpy. However, the values 7.8 and 5.5 are similar enough in magnitude to suggest that both T_{SS} and T_{AS} arrangements will be significant for Ru-tpy, even if the former arrangement with tpy ligands oriented towards the same strand will predominate. Our results indicating a relatively modest cooperativity factor ($y = 2.8$) for Ru-tpy appears to be in contrast to the case of Ru(phen)$_2$dppz^{2+}, for which a rather substantial Δ–Λ cooperativity can be inferred, since Cardin and co-workers report that the hexamer duplex used in their crystal structure study preferentially binds precisely one Δ- and one Λ-Ru(phen)$_2$dppz in solution.[5e]

Experimental

Materials

All experiments were performed in aqueous solution (pH = 7.0) containing 150 mM NaCl and 1 mM cacodylate (dimethylarsinic acid sodium salt) except for the LD experiments where 10 mM NaCl was used (pH = 7.0). This was because a lower
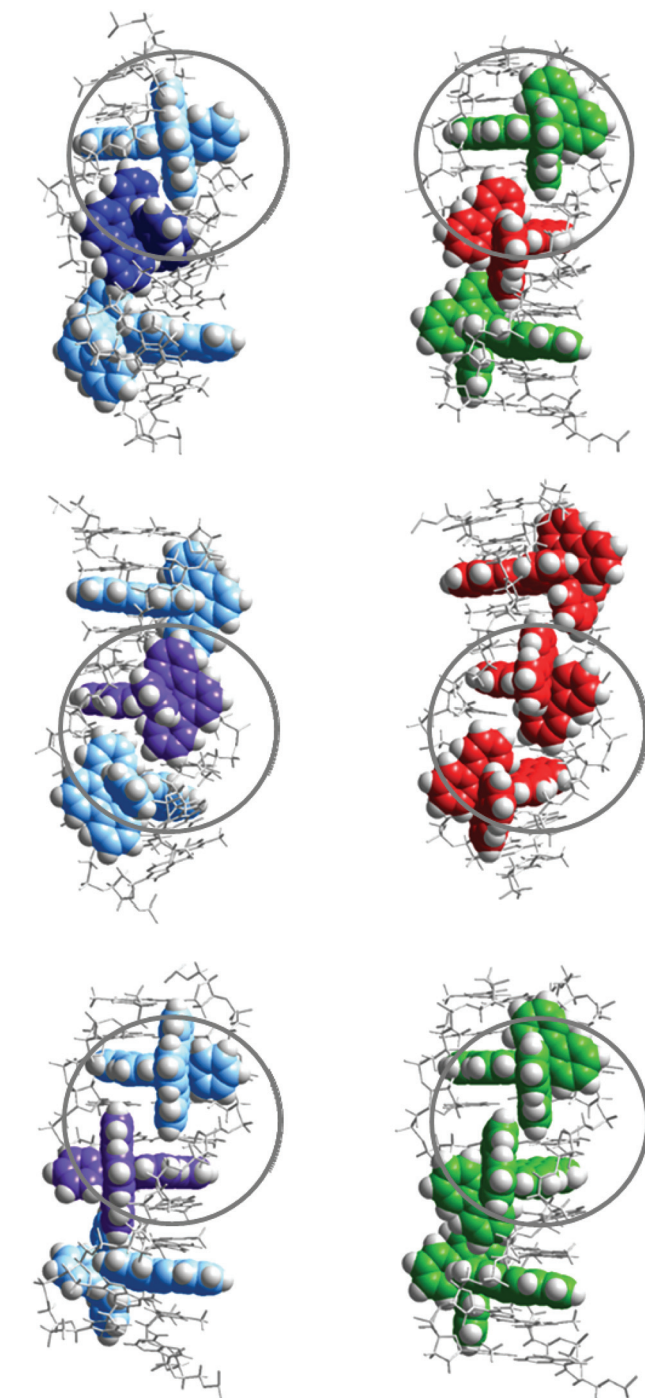
Fig. 10 Schematic illustration of the proposed interaction geometries for Ru-tpy (left) and the corresponding geometries of Δ- (green) and Λ- (red) Ru-bpy (right). Top row illustrates the "same-side" (T_{SS}) model while the middle and bottom row illustrate the "alternating side" (T_{AS}) model. Circles indicate similarities in intermolecular contacts. The models where constructed by manual docking and subsequent energy minimization in vacuum, using AMBER 2 force field in the HyperChem 8.0 software package (HyperCube, Inc.).

salt concentration gave a higher signal intensity without affecting the overall shape of the spectra. Stock solutions of calf thymus DNA (ctDNA) (~5 mM nucleotides) were prepared

by dissolving highly polymerized type I sodium salt calf thymus DNA (Sigma-Aldrich) in buffer. A stock solution of poly-(dAdT)$_2$ (AT-DNA) (∼5 mM nucleotides) was prepared by dissolving the sodium salt (Sigma-Aldrich) in buffer. The solutions were filtered two times through a 0.7 μm polycarbonate filter. Stock solutions of the complexes (∼1 mM) were prepared by dissolving the chloride salts in buffer. Concentrations were determined spectrophotometric using extinction coefficients: ε_{258} = 6600 M^{-1} cm^{-1} per nucleotide for ctDNA, ε_{260} = 6600 M^{-1} cm^{-1} per nucleotide for AT-DNA, ε_{371} = 16 900 M^{-1} cm^{-1} for Ru-tpy and ε_{444} = 16 100 M^{-1} cm^{-1} for Ru(bpy)$_2$dppz^{2+} (Ru-bpy). For ITC measurements the DNA solution was dialyzed against pure buffer for at least 48 hours at 8 °C. Ruthenium complex solutions of appropriate concentrations were prepared by dilution of the stock solutions in the dialysate. The dialysis membrane used had a molecular weight cut-off of 3.5–5 kDa (Spectra-Por® Float-A-Lyzer® G2, Sigma Aldrich).

Δ- and Λ-[Ru(bpy)$_2$dppz]Cl$_2$ used in this study were prepared as previously reported.[11a]

Other chemicals were purchased from Sigma-Aldrich and used without purification.

Synthesis of [Ru(tpy)(py)dppz]Cl$_2$

The synthetic route for preparation of [Ru(tpy)(py)dppz]Cl$_2$ is shown in Scheme 2. The procedure for preparation of Ru(tpy)-Cl$_3$ and [Ru(tpy)(dppz)Cl]Cl are in accordance to the methods previously reported by Zhou *et al.* and Leising *et al.*, respectively.[7a,14] [Ru(tpy)(dppz)(py)][PF$_6$]$_2$ was synthesized using the method previously described by Zhou *et al.* with some modifications. A portion of 0.0557 g of [Ru(tpy)(dppz)Cl]Cl and 0.0270 g of AgNO$_3$ were refluxed in 20 mL of ethanol–water (1 : 1) for 3 h under N$_2$(g). The solution was filtered after cooling and the filtrate was refluxed again under N$_2$ (g) for another 4 h, with 0.0101 g pyridine (py) added. The solution was left in a fridge over night for cooling. The next day the product was precipitated using KPF$_6$ dissolved in MilliQ water, left for a few hours, collected on a filter, and washed with ethanol–ether (1 : 2). Purification of [Ru(tpy)(dppz)(py)][PF$_6$]$_2$ was done using column chromatography with CH$_3$CN and

neutral Al$_2$O$_3$. The eluate containing the pure orange product was collected leaving a dark purple residue layer on top of the column.

To replace the hexafluorophosphate anion with chloride, the CH$_3$CN solution of [Ru(tpy)(dppz)(py)](PF$_6$)$_2$ was reduced to ∼1 mL evaporating with a stream of N$_2$ under mild heating, where after 0.5 g of ([CH$_3$(CH$_2$)$_3$]$_4$NCl), dissolved in 1 mL of acetone, was added in increasing portions while stirring until the solution was only weakly yellow and the precipitation complete. The product was collected by a sintered glass filter and washed first with acetone and then with diethyl ether to yield [Ru(tpy)(dppz)(py)]Cl$_2$ as a brown powder (36%, calculated from the starting material, Ru(tpy)Cl$_3$). UV/vis (in water; λ_{max} in nm, $\varepsilon/10^3$ M^{-1} cm^{-1} enclosed in parenthesis): 475(12.1), 372(16.9), 310(45.4), 275(69.2). ^{1}H NMR (as PF$_6$ salt, 400 MHz, acetone-d_6): δ 10.03 (dd, J = 8.2, 1.3 Hz, 1H), 9.56–9.52 (m, 1H), 9.48 (dd, J = 5.4, 1.4 Hz, 1H), 8.94 (t, J = 8.0 Hz, 2H), 8.84–8.71 (m, 2H), 8.59–8.42 (m, 4H), 8.26–8.11 (m, 9H), 8.04–7.94 (m, 2H), 7.76 (ddd, J = 8.2, 5.5, 0.8 Hz, 1H), 7.49–7.42 (m, 3H). The ^{1}H NMR spectrum of Ru-tpy (see Fig. S8 in ESI†) was in accordance with previous results by Zhou *et al.* (2009)[7a] and showed no significant impurities.

Spectroscopy

Absorption spectra were measured on a Varian Cary 4000 UV/vis spectrophotometer (path length = 1 cm). The reverse absorption titration spectra for Ru-tpy were measured with a constant concentration of 5 μM Ru-tpy in buffer. The stock solution of AT-DNA (with 5 μM of Ru-tpy to avoid dilution) added directly in the cuvette (path length = 1 cm) in aliquots up to a concentration of 80 μM nucleotides.

Linear dichroism spectra (LD) were measured on a Chirascan LD spectropolarimeter on samples oriented in an outer-rotating Couette flow cell with a 1 mm path length at a rate of 1000 rpm. The spectra of the same samples were recorded without rotation for baseline contribution and were subsequently subtracted from the LD spectra. The concentration of ctDNA used in the measurements was 266 μM nucleotides and mixed with complex solution with appropriate concentration to obtain desired [Ru]/[base pairs] ratios. Circular dichroism (CD) spectra were recorded on a Chirascan CD spectropolarimeter similarly as the absorption spectra. Five CD spectra were averaged for each sample. To be consistent with the absorption and ITC measurements, AT-DNA was used for the CD measurements (∼138 μM nucleotides).

Calorimetric data was obtained using an ITC200 isothermal titration calorimeter (Microcal) controlled by Origin 7.0 software. The ruthenium complexes (∼600 μM) were loaded in a syringe (40 μL) and titrated in 2 μl aliquots into 206 μl of AT-DNA in 150 mM NaCl aqueous solution (∼340 μM nucleotides). By integrating the power required to maintain the reference and sample cells at the same temperature it is possible to obtain a direct measurement of the heat generated or absorbed when complex and DNA interact. The experimental raw data consists of a series of heat flow peaks, and each peak
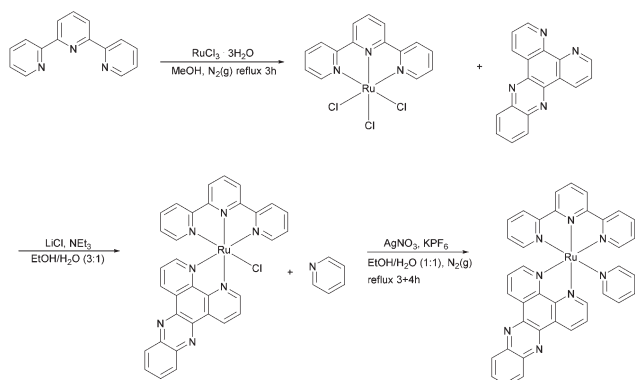
Scheme 2 Synthesis of Ru-tpy.

corresponds to one injection of complex. These heat flow spikes are integrated with respect to time, which gives the total heat exchanged per mole injectant, plotted against the ratio [Ru]/[base pairs]. The primary ITC data was corrected for the heat of ligand dilution by subtracting the average heat per injection of complex titrated into buffer. There was negligible heat arising from DNA dilution. The experiments were performed at 20 °C, 25 °C and 30 °C.

^{1}H NMR spectrum of $[Ru(tpy)(py)dppz](PF_6)_2$ in acetone-d_6 was recorded on an Agilent 400 MHz spectrophotometer.

Theory and methods

Analysis of LD spectra

The isotropic absorption spectrum A_{iso} of a sample can be considered as a simple sum of component spectral envelopes e_i, each such envelope itself being a collecting all electronic transitions with a common polarisation direction relative to the molecular coordinate system:

$$A_{iso} = \sum_i e_i \tag{1}$$

Then, the linear dichroism spectrum LD will be a weighted sum of the same component spectral envelopes:

$$LD = \sum_i w_i e_i \tag{2}$$

there for an effectively uniaxial oriented system (*e.g.* DNA oriented by the shear flow in a Couette cell) the weights w_i are determined by the orientation of the polarization direction characteristic for the electronic transition dipole moments of e_i relative to the macroscopic orientation axis of the system:

$$w_i = \gamma \frac{3}{2} S(3 \cos^2 \theta_i - 1) \quad 0 \leq S \leq 1 \tag{3}$$

where γ is the ratio of the optical path-length of the LD to the absorption measurement, θ_i is the angle between the transition dipole moment direction of envelope e_i and the orientation axis of the molecular system (in our case the DNA helix axis), and the orientation factor S describes the degree of alignment of the molecular system orientation axis relative to the macroscopic orientation axis, with $S = 0$ for an unoriented and $S = 1$ for a perfectly aligned sample.

The reduced linear dichroism LD^r value at a certain wavelength is defined as the ratio of the linear dichroism value over the isotropic absorbance value:

$$LD^r = \frac{LD}{A_{iso}} \tag{4}$$

In wavelength regions where a single component spectral envelope e_i dominates the absorption spectrum, the LD^r curve will be essentially constant and take the value w_i, *e.g.* as observed around the 260 nm band of B-DNA. Since θ for the

in-plane polarized $\pi \rightarrow \pi^*$ nucleobase transitions here is close to 90°, the orientation factor S_0 for ligand-free DNA can readily be calculated from the LD^r value.

$$LD_{260}^r = w = -\gamma \frac{3}{2} S_0 \tag{5}$$

However, in most cases, and in particular for 3D-chromophores like ruthenium polypyridyl complexes, component spectral envelopes overlap substantially over the whole range of the spectrum, and the LD^r curve will vary strongly with wavelength. Deconvolution of the experimental A_{iso} and LD spectra into component envelopes, and thereby determining the weights w_i, can in favorable cases be accomplished by the TEM-method.[5a,15] For a system with two component envelope spectra, having distinct characteristic absorption band features and distinct weights, the TEM-method in matrix notation can be formulated as the solution of the combined eqn (1) and (2):

$$\begin{bmatrix} \mathbf{a} & \mathbf{b} \end{bmatrix} \begin{bmatrix} 1 & w_1 \\ 1 & w_2 \end{bmatrix}^{-1} = \begin{bmatrix} \mathbf{e_1} & \mathbf{e_2} \end{bmatrix} \tag{6}$$

where $\mathbf{a}$, $\mathbf{b}$, $\mathbf{e_1}$ and $\mathbf{e_2}$ are column vectors corresponding to the isotropic absorption, linear dichroism and the two component envelope spectra, respectively. The variables w_1 and w_2 in eqn (6) are varied until, as determined by visual inspection, the characteristic features of component $\mathbf{e_2}$ have vanished in component $\mathbf{e_1}$ and *vice versa*.

The orientation factor S is required for the angular orientation to be determined from the weights w_i. For a dye that (a) is strongly bound to DNA; (b) has significant absorption at wavelengths >300 nm (where the DNA is transparent); and (c) has, within a certain range of [dye]/[DNA] ratios, invariant binding geometry and invariant absorption spectrum; S can readily be obtained as follows:

Let two LD spectra with different [dye]/[DNA] ratios (within the invariant range) be column vectors $\mathbf{L_1}$ and $\mathbf{L_2}$, and $\mathbf{L_0}$ be the LD spectrum of a sample with DNA only. Then, if condition (c) is fulfilled, the three columns are linearly dependent, thus scalars α and β can be found so that $\alpha \mathbf{L_1} + \beta \mathbf{L_2} = \mathbf{L_0}$; in matrix notation:

$$\mathbf{Mx} = \mathbf{L_0} \tag{7}$$

where $\mathbf{M} = [\mathbf{L_1} \ \mathbf{L_2}]$ and $\mathbf{x} = [\alpha; \beta]$. Solving eqn (7) by a least square projection gives α and β:

$$(\mathbf{M^T M})^{-1} \mathbf{M^T L_0} = \mathbf{x} \tag{8}$$

When condition (a) is fulfilled, practically all added dye can be considered to be bound; and with the DNA concentration being equal in the three samples, the vectors can be written as:

$$\mathbf{L_0} = \gamma S_0 \mathbf{d} \quad \mathbf{L_1} = \gamma S_1 (\mathbf{d} + c_1 \mathbf{b}) \quad \mathbf{L_2} = \gamma S_2 (\mathbf{d} + c_2 \mathbf{b}) \tag{9}$$

where (with $\gamma = 1$), $\mathbf{d}$ is the LD spectrum at perfect orientation of DNA only, $\mathbf{b}$ is the LD spectrum at perfect orientation of bound dye at unit concentration, and c_1 and c_2 are

the two known total dye concentrations. Since condition (b) assures that $\mathbf{d}$ is zero and $\mathbf{b}$ is non-zero for wavelengths > 300 nm, the following two equations are obtained by inserting eqn (9) in (7):

$$\alpha S_1 + \beta S_2 = S_0 \quad c_1 \alpha S_1 + c_2 \beta S_2 = 0 \quad (10)$$

Since γS_0 can be evaluated from eqn (5), S_1 and S_2 can be obtained from known quantities after solving the two equations in (10):

$$S_1 = \frac{S_0 c_2}{\alpha(c_2 - c_1)} \quad S_2 = \frac{S_0 c_1}{\beta(c_2 - c_1)} \quad (11)$$

Analysis of binding isotherms

Although global fitting of calorimetric and excited state life-time data for Δ- and Λ-Ru-bpy and their 1,10-phenanthroline analogues required a fairly complicated binding model comprising a symmetrical and a pair of unsymmetrical intercalation geometries (Model 3), fits to calorimetric data only were found to be satisfactory with a model with a single binding geometry.[10] This model, the classical McGhee–von Hippel single ligand cooperative binding model was used also in this work, and involves three adjustable parameters: the thermodynamic binding constant K, the binding site coverage parameter n and the cooperativity factor y.[16] Given values of these three parameters (assumed to be constant in the small temperature range used here), and total concentrations of binding sites $[\mathrm{B}]_{\mathrm{tot}}$ (*i.e.* base pairs) and DNA-ligand $[\mathrm{L}]_{\mathrm{tot}}$ (*i.e.* ruthenium complex) for each step of the titration, the mass-balance equations were solved iteratively with a Newton–Raphson procedure, to give consistent binding densities θ and free ligand concentrations $[\mathrm{L}]_{\mathrm{free}}$, as well as the conditional probabilities p_{ij}, as previously described.[10,17]

Calorimetric titration

The ITC data obtained at a certain temperature was assumed to be composed of three components:

$$\mathrm{ITC}(i) = (\Delta H^{\circ}_{\mathrm{b}})\Delta\mathbf{b}(i) + (\Delta H^{\circ}_{\mathrm{nn}})\Delta\mathbf{nn}(i) + \Delta H_{\mathrm{baseline}} \quad (12)$$

where $\Delta H^{\circ}_{\mathrm{b}}$ is the standard binding enthalpy change, $\Delta H^{\circ}_{\mathrm{nn}}$ is the standard nearest neighbor interaction enthalpy change and $\Delta H_{\mathrm{baseline}}$ is a small constant value. For titration data point i, the change in concentration of bound ligand $\Delta\mathbf{b}(i)$ is calculated as $[\mathrm{B}]_{\mathrm{tot}}(i)[\theta(i) - \theta(i - 1)]$ and the change in concentration of nearest neighbors $\Delta\mathbf{nn}(i)$ is calculated as $[\mathrm{B}]_{\mathrm{tot}}(i)[\theta(i)p_{22}(i) - \theta(i - 1)p_{22}(i - 1)]$, where p_{22} is the conditional probability that a bound ligand is followed by another bound ligand on the DNA lattice. The ΔH values were determined by projecting the matrix with the ITC data as columns, one for each temperature, on the space spanned by the $\Delta\mathbf{b}$, $\Delta\mathbf{nn}$ and a constant vector. The simulated ITC curves were then calculated with eqn (12) and the goodness-of-fit determined as the Euclidian norm of the difference between the measured and simulated data matrices.

Spectroscopic titration

The absorption spectra were arranged in data matrix $\mathbf{M}$ as columns with w elements corresponding to the wavelengths recorded; the columns corresponding to the t titration steps. Singular value decomposition, using the *svd* command in the MATLAB software, factorized the data matrix into two matrices of orthonormal columns $\mathbf{U}$ and $\mathbf{V}$, and a diagonal matrix $\mathbf{S}$ with the singular values $s_1 \geq s_2 \geq s_3 \cdots \geq 0$ along the diagonal. Keeping only the m singular values that are significantly larger than zero make it possible to simplify the factorization:

$$\mathbf{M} = \mathbf{U}\mathbf{S}\mathbf{V}^{\mathrm{T}} = \underline{U}\underline{S}\underline{V}^{\mathrm{T}} + \mathbf{N} \quad (13)$$

where $\underline{S}$ is the upper m by m submatrix of $\mathbf{S}$; $\underline{U}$ and $\underline{V}$ are the first m columns of $\mathbf{U}$ and $\mathbf{V}$, respectively, and $\mathbf{N}$ is a matrix of small elements, ideally corresponding only to the noise in the measurements. Assuming thus that the titration involves m different absorbing species, with absorption spectra in w by m matrix $\mathbf{A}$ and concentrations in t by m matrix $\mathbf{C}$, the factorization can now be written as

$$\mathbf{M} - \mathbf{N} = \underline{U}\underline{S}\underline{V}^{\mathrm{T}} = \mathbf{A}\mathbf{C}^{\mathrm{T}} = \underline{U}[\mathbf{R}\mathbf{R}^{-1}]\underline{S}\underline{V}^{\mathrm{T}} = [\underline{U}\mathbf{R}][\mathbf{R}^{-1}\underline{S}\underline{V}^{\mathrm{T}}] \quad (14)$$

where $\mathbf{R}$ is a non-singular m by m matrix. Since $\mathbf{A} = \underline{U}\mathbf{R}$ and $\mathbf{C} = \underline{V}\underline{S}(\mathbf{R}^{-1})^{\mathrm{T}}$, any theoretical binding model, which can calculate a matrix $\mathbf{C}_{\mathrm{m}}$ of concentrations of m species, can be evaluated for consistency with the data by finding the $\mathbf{R}$ that is the least square projection of $\underline{V}\underline{S}$ on the space spanned by $\mathbf{C}_{\mathrm{m}}$:

$$\mathbf{R}^{\mathrm{T}} = (\mathbf{C}_{\mathrm{m}}^{\mathrm{T}}\mathbf{C}_{\mathrm{m}})^{-1}\mathbf{C}_{\mathrm{m}}^{\mathrm{T}}\underline{V}\underline{S} \quad (15)$$

By varying the adjustable parameters of the theoretical model, $\mathbf{C}_{\mathrm{m}}$ is varied to minimize the norm of the residual $\underline{V}\underline{S} - \mathbf{C}_{\mathrm{m}}\mathbf{R}^{\mathrm{T}}$ while keeping the specie spectra in $\mathbf{A} = \underline{U}\mathbf{R}$ physically reasonable (non-negative in the case of absorption spectra). In the present case, the concentration matrix $\mathbf{C}_{\mathrm{m}}$ was constructed with three columns corresponding to free ligand, bound ligand with a neighboring free binding site, calculated as $[\mathrm{B}]_{\mathrm{tot}}\theta(1 - p_{22})$, and bound ligand adjacent to another bound ligand, calculated as $[\mathrm{B}]_{\mathrm{tot}}\theta p_{22}$.

Conclusion

The angular orientation of the dppz and tpy ligands as determined by LD and CD spectroscopies, strongly indicate that Ru-tpy binds from the minor groove by intercalating the dppz ligand between the base pairs, as has previously been determined for the isomeric complexes Δ- and ΛRu-bpy. The strong hypochromicity in the dppz absorption band is almost identical in magnitude to that of ΔRu-bpy, indicating that the alignment in the intercalation pocket is similar, too.

A simple cooperative binding model with one symmetrical binding geometry provide an excellent fit to data for calorimetric and absorption titrations of Ru-tpy into AT-DNA. The intrinsic intercalation has an equilibrium constant of 10^6 M^{-1}, close to that of Δ-Ru-bpy, and is associated with a small endothermic enthalpy change of +3 kJ M^{-1}. The cooperativity

factor is 2.8, and the associated neighbor interaction enthalpy is exothermic, -10.2 kJ M^{-1}; these values being in-between those of Δ- and Λ-Ru-bpy, and consistent with a slight preference of a one-sided arrangement of tpy-ligands of complexes consecutively bound to DNA.

Acknowledgements

Notes and references

1 S. M. Cohen and S. J. Lippard, *Prog. Nucleic Acid Res. Mol. Biol.*, 2001, **67**, 93–130.

2 (*a*) J. K. Barton, A. T. Danishefsky and J. M. Goldberg, *J. Am. Chem. Soc.*, 1984, **106**, 2172–2176; (*b*) J. K. Barton, J. M. Goldberg, C. V. Kumar and N. J. Turro, *J. Am. Chem. Soc.*, 1986, **108**, 2081–2088.

3 (*a*) Y. Jenkins, A. E. Friedman, N. J. Turro and J. K. Barton, *Biochemistry*, 1992, **31**, 10809–10816; (*b*) C. Hiort, P. Lincoln and B. Nordén, *J. Am. Chem. Soc.*, 1993, **115**, 3448–3454; (*c*) A. E. Friedman, J. C. Chambron, J. P. Sauvage, N. J. Turro and J. K. Barton, *J. Am. Chem. Soc.*, 1990, **112**, 4960–4962.

4 C. G. Hartinger, S. Zorbas-Seifried, M. A. Jakupec, B. Kynast, H. Zorbast and B. K. Keppler, *J. Inorg. Biochem.*, 2006, **100**, 891–894.

5 (*a*) P. Lincoln, A. Broo and B. Nordén, *J. Am. Chem. Soc.*, 1996, **118**, 2644–2653; (*b*) R. Hartshorn and J. Barton, *J. Am. Chem. Soc.*, 1992, **114**, 5919–5925; (*c*) I. Haq, P. Lincoln, D. C. Suh, B. Nordén, B. Z. Chowdry and J. B. Chaires, *J. Am. Chem. Soc.*, 1995, **117**, 4788–4796; (*d*) H. Song, J. T. Kaiser and J. K. Barton, *Nat. Chem.*, 2012, **4**, 615–620; (*e*) J. P. Hall, D. Cook, S. R. Morte, P. McIntyre, K. Buchner, H. Beer, D. J. Cardin, J. A. Brazier, G. Winter, J. M. Kelly and C. J. Cardin, *J. Am. Chem. Soc.*, 2013, **135**, 12652–12659; (*f*) H. Niyazi, J. P. Hall, K. O'Sullivan, G. Winters, T. Sorenson, J. M. Kelly and C. J. Cardin, *Nat. Chem.*, 2012, **4**, 621–628.

6 (*a*) H. H. Thorp, *J. Inorg. Organomet. Polym.*, 1993, **3**, 41–57; (*b*) J. G. Goll and H. H. Thorp, *Inorg. Chim. Acta*, 1996, **242**, 219–223; (*c*) P. J. Carter, C. C. Cheng and H. H. Thorp, *J. Am. Chem. Soc.*, 1998, **120**, 632–642; (*d*) B. T. Farrer and H. H. Thorp, *Inorg. Chem.*, 2000, **39**, 44–49; (*e*) N. Grover, N. Gupta, P. Singh and H. H. Thorp, *Inorg. Chem.*, 1992, **31**, 2014–2020.

7 (*a*) Q. X. Zhou, F. Yang, W. H. Lei, J. R. Chen, C. Li, Y. J. Hou, X. C. Ai, J. P. Zhang, X. S. Wang and B. W. Zhang, *J. Phys. Chem. B*, 2009, **113**, 11521–11526; (*b*) D. Ossipov, S. Gohil and J. Chattopadhyaya, *J. Am. Chem. Soc.*, 2002, **124**, 13416–13433.

8 (*a*) M. Frasconi, Z. Liu, J. Lei, Y. Wu, E. Strekalova, D. Malin, M. W. Ambrogio, X. Chen, Y. Y. Botros, V. L. Cryns, J.-P. Sauvage and J. F. Stoddart, *J. Am. Chem. Soc.*, 2013, **135**, 11603–11613; (*b*) A. Bahreman, B. Limburg, M. A. Siegler, R. Koning, A. J. Koster and S. Bonnet, *Chem. – Eur. J.*, 2012, **18**, 10271–10280; (*c*) S. Bonnet, B. Limburg, J. D. Meeldijk, R. Gebbink and J. A. Killian, *J. Am. Chem. Soc.*, 2011, **133**, 252–261.

9 (*a*) K. K. Patel, E. A. Plummer, M. Darwish, A. Rodger and M. J. Hannon, *J. Inorg. Biochem.*, 2002, **91**, 220–229; (*b*) C. W. Jiang, H. Chao, H. Li and L. N. Ji, *J. Inorg. Biochem.*, 2003, **93**, 247–255; (*c*) H. Chao, W. J. Mei, Q. W. Huang and L. N. Ji, *J. Inorg. Biochem.*, 2002, **92**, 165–170.

10 J. Andersson, L. H. Fornander, M. Abrahamsson, E. Tuite, P. Nordell and P. Lincoln, *Inorg. Chem.*, 2013, **52**, 1151–1159.

11 (*a*) P. Lincoln and B. Nordén, *J. Phys. Chem. B*, 1998, **102**, 9583–9594; (*b*) S. Vasudevan, J. A. Smith, M. Wojdyla, A. DiTrapani, P. E. Kruger, T. McCabe, N. C. Fletcher, S. J. Quinn and J. M. Kelly, *Dalton Trans.*, 2010, **39**, 3990–3998; (*c*) T. Very, S. Despax, P. Hébraud, A. Monari and X. Assfeld, *Phys. Chem. Chem. Phys.*, 2012, **14**, 12496–12504.

12 (*a*) R. Siebert, F. Schlütter, A. Winter, M. Presselt, H. Görls, U. S. Schubert, B. Dietzek and J. Popp, *Cent. Eur. J. Chem.*, 2011, **9**, 990–999; (*b*) T. K. Aldridge, E. M. Stacy and D. R. McMillin, *Inorg. Chem.*, 1994, **33**, 722–727.

13 (*a*) R. Lyng, A. Rodger and B. Nordén, *Biopolymers*, 1991, **31**, 1709–1720; (*b*) R. Lyng, A. Rodger and B. Nordén, *Biopolymers*, 1992, **32**, 1201–1214.

14 R. A. Leising, S. A. Kubow, M. R. Churchill, L. A. Buttrey, J. W. Ziller and K. J. Takeuchi, *Inorg. Chem.*, 1990, **29**, 1306–1312.

15 J. Michl and E. Thulstrup, *Spectroscopy with Polarized Light*, VCH Publishers, New York, 1986, p. 120.

16 J. D. McGhee and P. H. V. Hippel, *J. Mol. Biol.*, 1974, **86**, 469–489.

17 P. Lincoln, *Chem. Phys. Lett.*, 1998, **288**, 647–656.